ChemPhysMater xxx (xxxx) xxx

Contents lists available at ScienceDirect

ChemPhysMater

journal homepage: https://www.keaipublishing.com/en/journals/chemphysmater/

Research Article

High-performance acoustic biocomposites: Castor oil-based polyurethane foam reinforced with rice husk-derived cellulose and silica

Nathapong Sukhawipat[a,b], Thitaree Phokasem[a], Nutcha Sukkun[a], Purintorn Chanlert[c,d], Wichain Chailad[e], Narongrit Sosa[f,g], Ziyin Xiang[h], Arreerat Jiamprasertboon[f,g], Kritsadi Thetpraphi[f,i,*]

[a] Novel and Advanced Sustainable Materials LAB, Department of Mechanical Engineering Technology, Collage of Industrial Technology, King Mongkut's University of Technology North Bangkok, Bangkok 10800, Thailand
[b] Operations Center of Aircraft and Defense Technology (CADeT), KMUTNB Techno Park, King Mongkut's University of Technology North Bangkok, Bangkok 10800, Thailand
[c] Program of Physics, Faculty of Science and Technology, Songkhla Rajabhat University, Mueang, Songkhla 90000, Thailand
[d] Research Unit in Applied Physics and Advanced Materials (APAM), Faculty of Science and Technology, Songkhla Rajabhat University, Mueang, Songkhla 90000, Thailand
[e] Department of Materials and Metallurgical Engineering, Faculty of Engineering, Rajamangala University of Technology Thanyaburi, Pathum Thani 12110, Thailand
[f] School of Science, Walailak University, Thasala, Nakhon Si Thammarat 80160, Thailand
[g] Functional Materials and Nanotechnology Center of Excellence, Walailak University, Nakhon Si Thammarat 80160, Thailand
[h] YuYao Innovation Institute, Zhejiang Wanli University, Ningbo 315402, China
[i] Research Center for Theoretical Simulation and Applied Research in Bioscience and Sensing, Walailak University, Nakhon Si Thammarat 80160, Thailand

ARTICLE INFO

Keywords:
Castor oil-based polyurethane foam
Bio-based polyurethane foam
Rice husk fillers
Sustainable acoustic absorption
Bio-based composites

ABSTRACT

The development of sustainable and high-performance acoustic materials requires replacing petroleum-based polyurethane foams (PUFs) with renewable alternatives. In this work, fully bio-based PUFs were synthesized using castor oil as polyol and reinforced with rice husk-derived silica (RHS) and cellulose (RHC). A series of formulations with varying additive loadings (0–2.0 phr) was fabricated and systematically characterized for chemical structure, morphology, thermal stability, mechanical strength, moisture resistance, and acoustic absorption. Results confirmed successful integration of silica–cellulose fillers within the castor oil-based polyurethane matrix, with Fourier-transform infrared spectroscopy indicating enhanced hydrogen bonding and filler–matrix interactions. The addition of RHS/RHC improved compressive strength and stiffness, with the optimum performance observed at 0.7–1.5 phr. Thermal analysis revealed enhanced degradation resistance at higher filler loadings, while moisture absorption tests showed reduced equilibrium uptake, particularly at ≥0.7 phr. Acoustic evaluation demonstrated that moderate filler contents preserved sound absorption performance comparable to that of neat PUF, while excessive loading reduced broadband absorption. Overall, the findings highlight the dual advantage of sustainable sourcing and functional property enhancement, positioning castor oil-based PUF reinforced with agro-waste fillers as a promising candidate for green acoustic and structural applications. Future work will explore replacing petroleum-based isocyanates with bio-derived or less-toxic alternatives, alongside filler ratio optimization, flammability and durability assessments, scalability, and environmental adaptability under humid conditions.

1. Introduction

The development of sustainable biomaterials has gained increasing attention in recent years, driven by the urgent need for environmentally friendly, high-performance alternatives in diverse advanced applications such as construction, packaging, biomedical devices, and acoustic control. Replacing petroleum-based materials with biocompatible, renewable, and cost-effective resources not only reduces dependence on fossil feedstocks but also contributes to carbon footprint reduction and circular economy strategies. Within this broader context, acoustic applications stand out, as noise pollution has become a critical environmental issue affecting human health, productivity, and quality of life. This dual challenge—enhancing material performance while addressing environmental concerns—underscores the importance of developing green sound-absorbing foams.

* Corresponding author.
E-mail address: kritsadi.th@wu.ac.th (K. Thetpraphi).

https://doi.org/10.1016/j.chphma.2026.03.007
Received 4 November 2025; Received in revised form 25 February 2026; Accepted 31 March 2026
Available online xxx
2772-5715/© 2026 The Authors. Publishing Services by Elsevier B.V. on behalf of KeAi Communications Co. Ltd. This is an open access article under the CC BY license (http://creativecommons.org/licenses/by/4.0/)

Please cite this article as: N. Sukhawipat, T. Phokasem, N. Sukkun et al., High-performance acoustic biocomposites: Castor oil-based polyurethane foam reinforced with rice husk-derived cellulose and silica, ChemPhysMater, https://doi.org/10.1016/j.chphma.2026.03.007

Conventional polyurethane foams (PUFs) are widely used as sound absorbers in construction and transportation due to their lightweight structure and tunable porosity [1–3]. However, the shortcomings of petroleum-derived PU foams have raised concerns about their long-term sustainability. These foams rely on petroleum-based polyols and toxic isocyanates, leading to drawbacks such as poor weatherability, flammability, high production cost, and dependence on nonrenewable resources. Their limited eco-compatibility and potential health hazards highlight the pressing need for bio-based alternatives. In this regard, biopolymers derived from cellulose and plant oils have shown great promise. For example, Szpiłyk et al. (2021) synthesized a biodegradable cellulose-derived polyol and demonstrated that the resulting PUF was not only thermally more resistant than conventional foams but also biodegradable in soil, with 70%–80% mass loss within 28 days [4]. Such findings underscore the transformative potential of bio-based polyols to address both performance and environmental challenges.

To address these issues, researchers have increasingly explored bio-based polyols derived from plant oils and agricultural residues. Plant oils such as soybean, rice, coconut, and castor oils are renewable, biodegradable, abundant, and relatively inexpensive. They also allow chemical modification to tailor hydroxyl functionality, enabling their effective use in PU synthesis [5]. Importantly, these bio-based systems offer reduced toxicity, potential for carbon neutrality, and alignment with global sustainability goals. For example, Kattiyaboota and Thongpina (2016) demonstrated the successful replacement of petroleum-based polyols with natural oil-based polyols for the synthesis of flexible PU foam [6]. Subsequent studies expanded the scope: Marcovicha et al. (2017) utilized palm oil-based polyols to achieve lower viscosity and stronger open-cell foams [7]; Yuvaraj L. et al. (2018) produced cost-effective closed-cell PUFs from castor oil-based polyols [8]; Patel et al. (2011) obtained a highly flame-retardant hyperbranched PU was synthesized by reacting tris(bisphenol-A) monophosphate with polypropylene glycol and castor oil, along with different diisocyanates [9]; and Riyapan et al. (2019) studied the potential of palm oil systems for closed-cell foam development [10]. The utilization of castor oil as a renewable polyol in PUF has attracted significant research interest due to its inherent cross-linking potential and environmental benefits. Recent studies by Shaik et al. (2021) [11] have explored one-step synthesis methods for stable castor oil-based foams, demonstrating their potential to completely replace synthetic polyols. To further enhance the structural stability of these bio-based matrices, researchers have explored the use of cross-linking agents like glycerol to reinstate foam growth and refine polymer phase morphology [12].

It has been found that among available natural oils, castor oil is especially attractive due to its high hydroxyl content, non-edible status, and global availability. While castor oil has emerged as a premier bio-polyol due to its high hydroxyl functionality and non-edible status, its application has been largely confined to rigid insulation foams. However, existing research has predominantly focused on single-oil polyol formulations and has seldom explored the incorporation of additives to achieve multifunctional performance. Moreover, most reported PUFs have been developed primarily for structural and engineering applications, such as construction and insulation, rather than for acoustic functionality. These foams are typically characterized by closed-cell morphologies, which inherently limit their sound-absorption effectiveness by promoting sound reflection rather than dissipation [13]. In contrast to conventional closed-cell bio-foams that promote sound reflection, our approach utilizes the synergistic interaction between the hybrid fillers and the castor oil matrix to facilitate cell-wall rupture, transforming the morphology into a highly dissipative open-cell network [14], thereby significantly enhancing acoustic absorption performance.

Rice husks—an abundant by-product of rice milling—represent a valuable source of both cellulose and silica. Incorporating these agro-waste derivatives into PUFs offers multiple advantages: mechanical reinforcement, an improved open-cell structure for acoustic absorption, and the valorization of agricultural residues that would otherwise pose disposal challenges. Beyond agro-waste fillers, silica-based additives have also been widely studied for their role in improving foam performance. Lee et al. (2022) demonstrated that incorporating 3 wt% silica nanoparticles into PUFs significantly enhanced both thermal insulation and mechanical properties, while silica aerogels further improved thermal conductivity control [15]. Similarly, Merillas et al. (2022) reported that silica aerogels within PUF scaffolds influenced cell size, mechanical properties, and thermal insulation, underscoring the critical role of pore architecture in optimizing these properties [16]. In addition to matrix development, the integration of functional fillers remains a vital strategy for enhancing foam performance. Recent research has explored the use of hollow glass microspheres to increase the loading capacity of nano-clays in flexible polyurethane foam, achieving a necessary balance between density and mechanical strength [17]. Progress in sustainable chemical synthesis is further evidenced by the development of auxetic polyurethane (APU) foams derived from castor oil (CO), which introduce unique mechanical properties through bio-based precursors [18]. Similarly, the application of halloysite nanoclay (HNC) as a bio-nanofiller at varying concentrations (1 wt%–5 wt%) has been shown to significantly improve the thermal stability, mechanical integrity, and sound absorption capabilities of flexible PUF [19]. Together, these advancements highlight the necessity of optimizing the filler-matrix interface to produce high-performance, sustainable acoustic solutions.

Previous investigations into bio-based polyurethane foams have generally followed two independent strategies. For example, Shaik et al. [11] and Kattiyaboota and Thongpina [6] focused on replacing petroleum-derived polyols with plant-oil-based systems, primarily targeting sustainability and mechanical stability, but without specifically optimizing acoustic performance or pore architecture for sound dissipation. On the other hand, filler-based approaches—such as silica nanoparticle incorporation by Lee et al. [15] or halloysite nanoclay reinforcement reported by [19], demonstrated improved stiffness and thermal resistance; however, these systems often emphasized insulation or structural reinforcement rather than broadband acoustic absorption. In several cases, increased filler loading led to partial pore closure or densification, which can compromise sound absorption efficiency despite mechanical gains.

Consequently, achieving simultaneous acoustic enhancement and mechanical reinforcement within a sustainable matrix remains a key challenge. In contrast to these single-modification strategies, the present study integrates dual rice husk-derived waste streams—cellulose (fibrous reinforcement) and silica (particulate stabilization) into a castor oil-based polyurethane system. By maintaining a controlled hybrid baseline and systematically varying total filler loading, this work demonstrates acoustic–mechanical synergy, where pore refinement enhances compressive strength and thermal stability without sacrificing open-cell characteristics essential for effective sound absorption.

To address this knowledge gap, this study develops castor oil-based polyurethane foams reinforced with cellulose and silica derived from rice husks. The NCO index of the PUFs was set to 100. The cellulose-to-silica ratio was fixed at 50:50 as a baseline composition selected to balance fibrous reinforcement (cellulose) and particulate stabilization (silica). Therefore, the term “optimal” in this work refers to the optimum total filler loading (phr) within this fixed baseline ratio. The total hybrid additive content was varied from 0 to 2.0 phr to systematically evaluate mechanical properties, morphology, thermal behavior, moisture resistance, and sound absorption. By utilizing renewable and low-cost feedstocks, this study clarifies the structure–property relationships governing acoustic–mechanical synergy in sustainable polyurethane foams.

2. Materials and methods

2.1. Polyurethane foam synthesis

The castor oil (CO), a natural polyol for polyurethane foam (PUF) substrate, was provided by Siripanit Industrial in Pathum Thani

Province, Thailand, with a molecular weight of 933.4 g/mol, a hydroxyl value of 160 mg KOH/g, and an acid value of 2.0 mg KOH/g. Chemicals such as hydrogen peroxide (H_2O_2, 35%) and sodium hydrogen carbonate ($NaHCO_3$, >90%) were obtained from Ajax Finechem (Sydney, Australia). Formic acid (HCOOH, 98%) came from Fisher Chemical (Shanghai, China). Ethyl acetate ($CH_3COOC_2H_5$, >99%) was supplied by RCI Lab-Scan Limited (Bangkok, Thailand). Polymeric diphenylmethane diisocyanate (PMDI, 31.5% NCO content, functionality = 2.7) was sourced from BASF (Ludwigshafen, Germany). DBTL (T-12 dibutyltin dilaurate, 95%) was purchased from Fluka Chemie AG (Darmstadt, Germany). Dabco 33-LV (33% triethylene diamine in propylene glycol) was acquired from Evonik Goldschmidt GmbH (Essen, Germany). Lastly, the amino acid silicone surfactant (Siwell-Reborn®RB-8084) was supplied by Guangdong Rebon Advanced Materials Co., Ltd. (Guangdong, China). The method to yield polyol from natural plant-based oils was modified from previous research [3,20,21].

2.2. Rice husk silica and cellulose preparation

Rice husk (RH) was collected from areas near Walailak University, Nakhon Si Thammarat, Thailand. The method of powder production and the materials derived from RH have been reproduced from the literature [22]. The husks were washed thoroughly with tap water and dried in an air-flow oven at 80 °C overnight. A 150 g portion of the pre-dried RH was treated with 0.20 M NaOH solution at 80 °C for 1 h. The mixture was filtered to separate the treated RH residue from the resulting dark-brown filtrate. The solid residue was subjected to repeated NaOH treatment and filtration. The dark-brown filtrate was subsequently acidified with 1.00 M HCl to precipitate rice husk silica (RHS). The obtained silica was washed with tap water until neutral pH and dried at 80 °C overnight. In parallel, the RH residue (150 g) was bleached with 6 wt.% NaOCl at 80 °C for 1 h, washed with tap water until neutral pH, and dried at 80°C overnight, yielding a light-yellow material identified as RH-derived cellulose or rice husk cellulose (RHC). Finally, both RHS and RHC were grounded into fine powders for subsequent use as composite fillers.

2.3. Preparation of CO-based PUF/RHS and RHC composite

In preparing the polyurethane foam, the NCO index was maintained at 100. The specified mixtures are presented in Table S1- Supplementary Information, which indicates the chemical composition used in the process. This study was designed as a foundational investigation to evaluate the feasibility of the hybrid system. A fixed 50:50 cellulose-to-silica mass ratio was selected as an initial baseline composition to balance the reinforcing effect of cellulose fibers with the stabilizing effect of silica particles, while minimizing compositional complexity in this first-phase study. Cellulose provides fibrous reinforcement and abundant hydroxyl groups that enhance hydrogen bonding with the polyurethane matrix, whereas silica contributes particulate stabilization, pore refinement, and improved thermal resistance. By fixing this hybrid ratio, the experimental design isolates the effect of total filler loading (phr) on composite performance without introducing additional compositional variables. Therefore, the term “optimal” in this study refers to the optimum total hybrid filler loading within this fixed 50:50 baseline ratio. The total hybrid filler content was varied as follows: 0, 0.3, 0.5, 0.7, 1.0, 1.5, and 2.0 phr. The foam was produced at room temperature (30–35 °C) using a magnetic stirrer set at 1400 rpm. Initially, the chemicals were divided into two parts (Fig. 1): the first containing castor oil, water, RB-8084, DBTL, and Dabco 33-LV; the second containing PMDI, RHS, and RHC. These parts were stirred separately for 20 minutes. After stirring, the first part was added to the second, and mixing continued until the foam reached a viscous, creamy consistency. The foam was then poured into a sealed mold measuring $13 \times 13 \times 13\,cm^3$ and left to rise for 3 min. To ensure complete polymerization, the PUF composites were cured in an oven at 60 °C for 24 h.

2.4. Characterization techniques

Chemical structure analysis

The chemical structure of CO was determined by ^1H NMR spectroscopy on a Bruker 400 Fourier transform spectrometer operating at 400.13 and 100.62 MHz. TMS served as the internal standard, and $CDCl_3$ was used as the solvent for sample dissolution. FTIR spectra of all samples were collected using a Perkin Elmer Universal ATR Sampling Accessory, Model Frontier, equipped with a Diamond/KRS-5 crystal as the ATR component. The samples were positioned on the crystal surface, and the pressure arm was calibrated until the force gauge indicated a force between 100 and 120 N. The spectral scan ranged from 4000 to $400\,cm^{-1}$, with 16 accumulations and a resolution of $4\,cm^{-1}$.

Thermal properties

Thermal gravimetry analysis (TGA) using TA Instruments SPT 2960 simultaneous DSC-TGA was performed to study the thermal properties. Samples weighing between 8 and 13 mg were heated from 30 to 800 °C under nitrogen at a rate of 10 °C/min. It should be noted that TGA measurements were performed only on the developed bio-based PUF formulations, as the primary objective of this study is to investigate formulation–property relationships within the castor-oil-based system.

Mechanical properties

The density of the PUF composites was assessed in accordance with ISO 4590-2002. Their dimensions were precisely measured with a Vernier calliper, and density was calculated using the formula density = mass/volume. For each foam formulation, six replicates ($n = 6$) with dimensions of $50 \times 50 \times 50\ mm^3$ are tested using a Testometric (M500-25AT) device on an Instron universal testing machine, following ISO 844-2007. The crosshead moved at a speed of 2.5 mm/min, and the compressive strength was determined at 20% deformation. Results from three replicates were averaged and expressed in kilopascals (kPa).

Morphology

The morphology of the PUF composites was analyzed using scanning electron microscopy (SEM) with a JSM-6510LV (JEOL, Japan) operated at 20.00 kV under high vacuum and high voltage conditions. Additionally, to observe the structure of WHF, an optical microscope with 4X magnification and a Xenon light source (DN-117M) (Nanjing Jiangnan Novel Optics, China) was employed. Additionally, the cell size distribution was performed using ImageJ software for analysis.

Moisture absorption study

The moisture absorption behavior of the PUF composites was evaluated in an in-situ controlled humidity chamber maintained at 80 ± 5% relative humidity at room temperature. This relative humidity level was chosen to reflect the average climatic conditions of Southeast Asia, where six regions of Thailand reported values ranging from 73.7% to 81.2% RH in 2024 [23]. For each formulation, five specimens were tested. The samples were weighed at 15-minute intervals for the first 5 h to assess short-term uptake, and were subsequently measured once daily for 21 days to evaluate long-term behavior. Moisture absorption was calculated as the percentage gain in mass relative to the initial dry weight.

The water absorption coefficient (A_w) in the linear region of water uptake was determined using Eq. (1) [24].

$$A_w = \frac{(M_i - M_0)}{A\sqrt{t}}. \quad (1)$$

Where is A cross-sectional surface area, t is the exposure time of the specimens in the controlled humidity chamber, and M_i and M_0 are mass specimens measured at the time t_i and t_0, respectively.

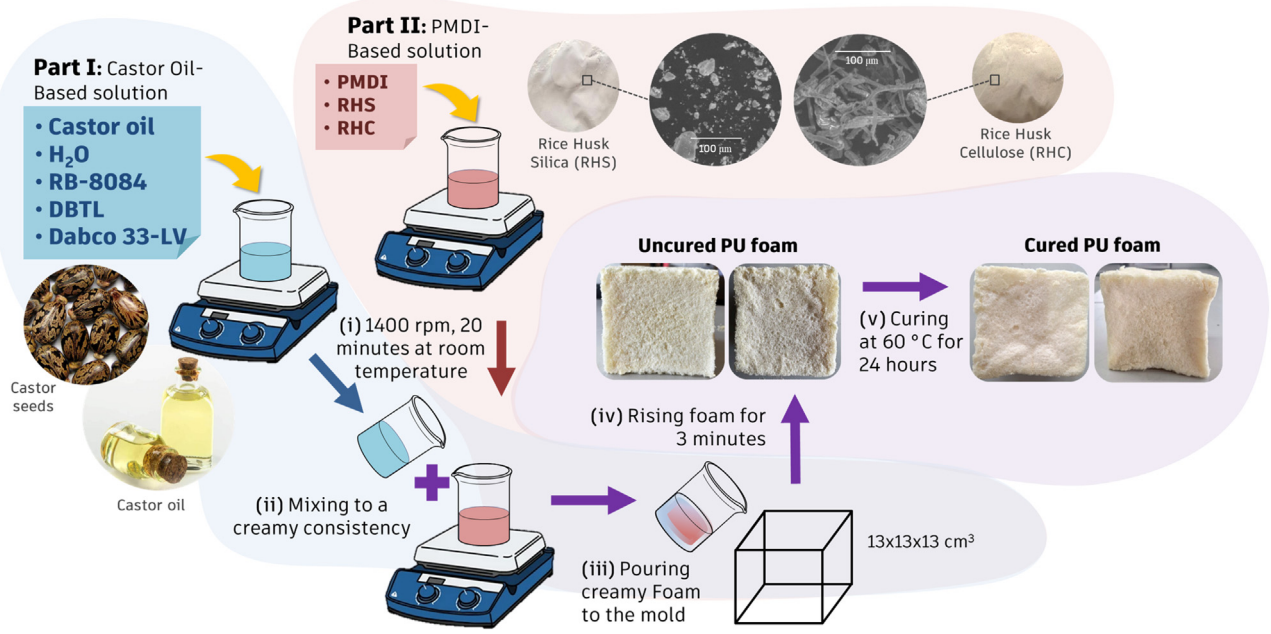

Fig. 1. The fabrication procedure of polyurethane foam (PUF) filled with rice husk silica (RHS) and rice husk cellulose (RHS).

Acoustic properties analysis

The normal-incidence sound absorption coefficient (SAC) of the samples was determined using the two-microphone impedance tube technique, following ASTM E1050 (1990) and ISO 10534-2 (1994) standards [25,26]. The impedance tube had an inner diameter of 28.6 mm and a length of 1000 mm. Each foam specimen was positioned in the sample holder at one end of the tube adjacent to the microphone channels, while a loudspeaker was mounted at the opposite end as the sound source. A commercial low-density petroleum-based polyurethane foam (≈0.09 g cm^{-3}) commonly used for acoustic applications was tested under identical conditions and included solely as a reference material for benchmarking acoustic performance. The comparison is limited to sound absorption behavior, as the scope of this work focuses on the formulation-dependent properties of the developed bio-based PUFs. Laboratory-grade $\frac{1}{4}$-inch microphones (GRAS 40PP; GRAS Sound & Vibration, Skovlunde, Denmark) were securely fitted into the microphone ports to capture the acoustic signals. The recorded data were transmitted to a computer via a data-acquisition system optimized for acoustic analysis (NI-9230; National Instruments, Austin, TX, USA). The SAC was calculated according to Eq. (2).

$$\mathrm{SAC} = 1 - \left| \frac{H_{12} - e^{-jk_0 s}}{e^{jk_0 s} - H_{12}} e^{2jk_0 x_1} \right|^2 . \tag{2}$$

Where H_{12} represents the transfer function between the two microphones, k_0 is the wave number, s is the spacing between Mic-1 and Mic-2, and x_1 is the distance between Mic-1 and the specimen surface. Data acquisition and signal processing were performed using a Python-based module.

3. Results and discussion

3.1. Polyurethane foam fabrication

Polyurethane foam (PUF) and PUF composites with varying silica–cellulose contents were successfully fabricated using a preparation process based on CO-derived PUF/RHS and RHC composites. As shown in Fig. 2, all formulations, ranging from neat PUF to those containing up to 2.0 phr of additive, exhibited uniform structure and stable form, confirming the effectiveness of the synthesis method. The resulting foams possess a desirable texture and exhibit environmentally friendly, potentially biocompatible properties, making them attractive for sustainable material development. With these qualities, the prepared PUF and PUF/silica–cellulose composites are promising candidates for various advanced applications, including construction, packaging, thermal insulation, and acoustic control.

3.2. Chemical structure analysis

The FTIR spectra of castor oil, cellulose, and silica were preliminarily analyzed to characterize their vibrational characteristics. As presented in Fig. 3(a)–(c), the FTIR spectra of castor oil (Fig. 3(a)) exhibited a broad band between 3470 and 3400 cm^{-1}, which was attributed to O–H stretching vibrations of hydroxyl groups on ricinoleic acid, which is the primary fatty acid component of castor oil derived from castor plant seeds [27]. Peaks at 2925 and 2855 cm^{-1} were assigned to the C–H stretching vibrations of aliphatic –CH_2 groups, while a weaker band at 3008 cm^{-1} corresponded to =C–H stretching from unsaturated chains. A strong absorption near 1740 cm^{-1} confirmed ester carbonyls from the triglyceride backbone, while the additional bands between 1160–1050 cm^{-1} were assigned to C–O stretching in ester linkages [28–30]. These features confirm the hydroxylated triglyceride structure of castor oil, which later participates in urethane bond formation.

Fig. 3(b) shows FT-IR spectrum of cellulose. It exhibited a broad O–H stretching envelope in the 3600–3200 cm^{-1} region, typical of extensive intra- and intermolecular hydrogen bonding in polysaccharides. The C–H stretching of glucopyranose units appeared around 2850 cm^{-1}. A broad band between 1650–1500 cm^{-1} was also observed, which was likely because of absorbed water and O–H bending. Strong peaks in the 1160–1050 cm^{-1} region and a distinct peak at 1030 cm^{-1} were associated with C–O–C and C–O stretching from β-1,4-glycosidic linkages of cellulose. A diagnostic band at 898 cm^{-1} confirmed β-glycosidic bonds, while additional peaks at 663 and 598 cm^{-1} corresponded to skeletal vibrations of the cellulose backbone [31–33].

The FTIR spectrum of silica (Fig. 3(c)) showed a weak, broad O–H stretching band between 3700–3200 cm^{-1}, which were attributed to surface silanol groups and adsorbed moisture. The weak intensity of this band is typical for silica, as the amount of surface hydroxyl groups depends strongly on drying history and surface area. In contrast, the

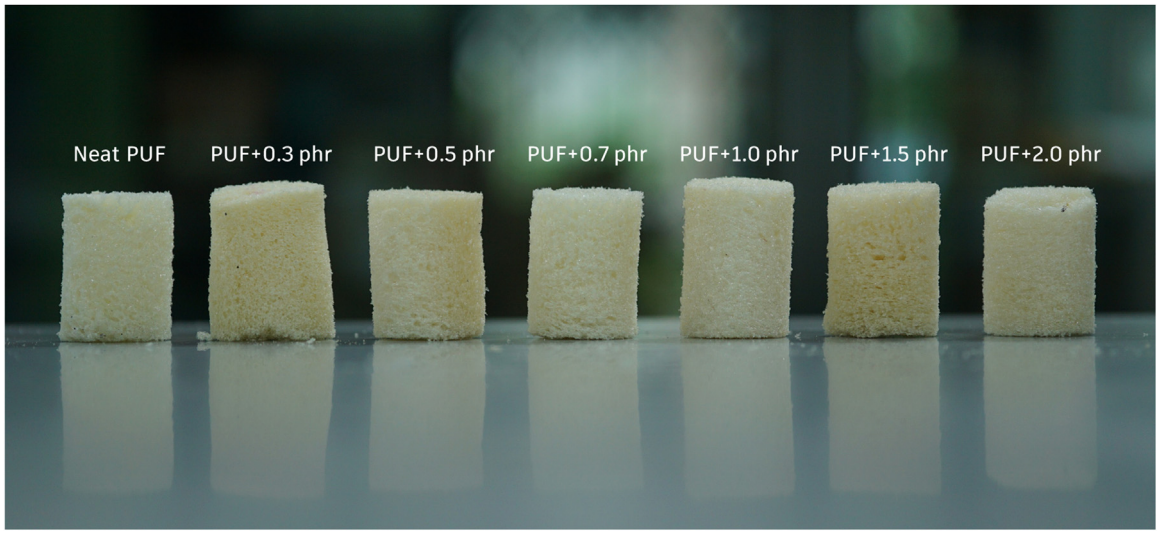

Fig. 2. Photographs of neat polyurethane foam (PUF) and PUF composites prepared with different silica–cellulose additive concentrations (0.3–2.0 phr) using the CO-based PUF/RHS and RHC composite process. All samples exhibit uniform texture and structural integrity, demonstrating the successful fabrication of environmentally friendly foams suitable for advanced applications.

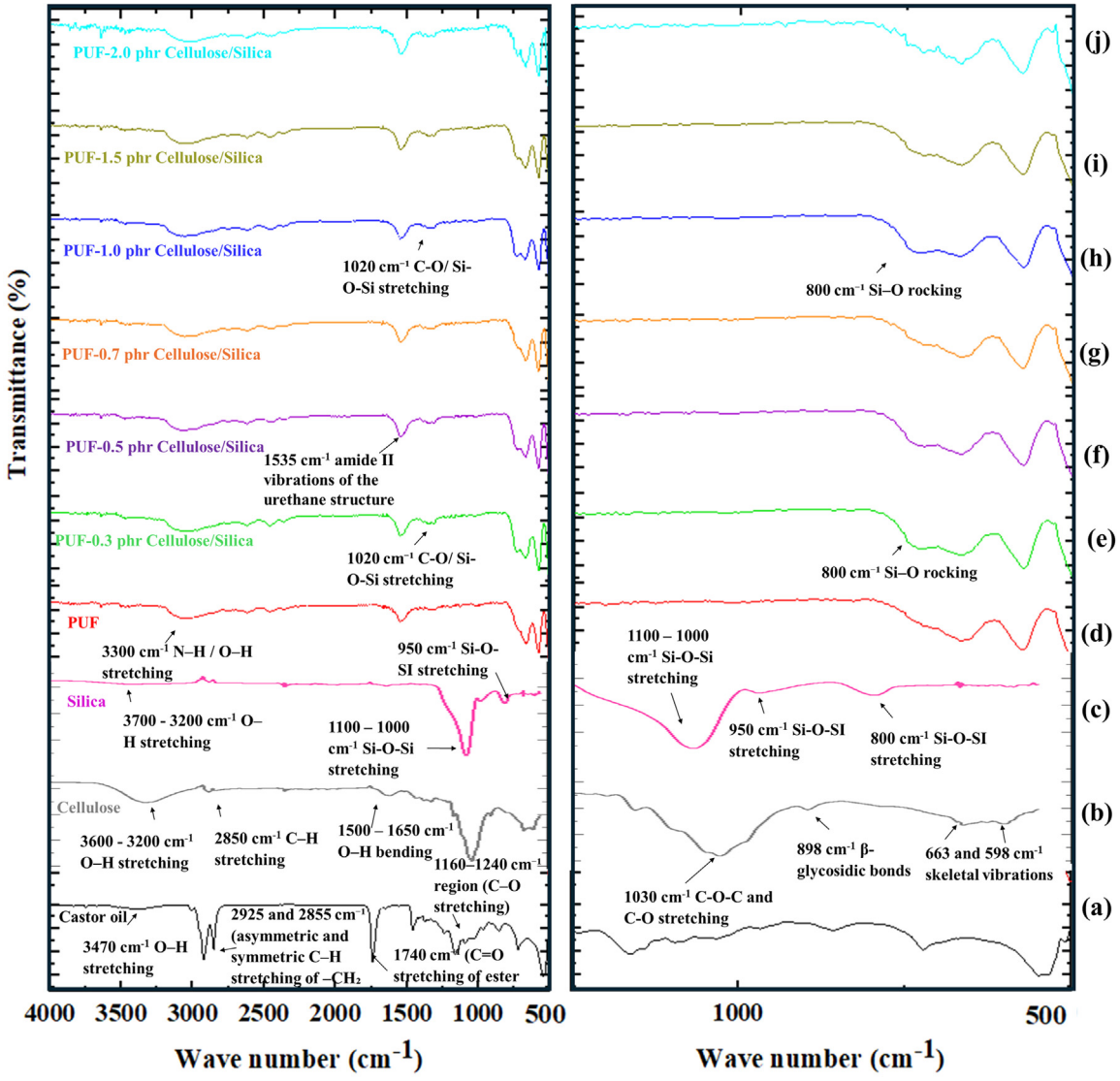

Fig. 3. FTIR spectra of (a) castor oil, (b) cellulose, (c) silica, (d) neat PUF (0 phr), and PUF composites filled with cellulose-silica at (e) 0.3 phr, (f) 0.5 phr, (g) 0.7 phr, (h) 1.0 phr, (i) 1.5 phr, and (j) 2.0 phr.

strongest absorption appeared in the 1100–1000 cm^{-1} region, assigned to asymmetric Si–O–Si stretching. A distinct band at 750–800 cm^{-1} corresponded to symmetric Si–O–Si stretching or rocking, while a shoulder near 950 cm^{-1} was linked to Si–OH stretching [34,35]. These well-defined bands serve as fingerprint peaks for silica and are particularly useful for identifying its occurrence within silica-cellulose-filled PUF composites.

After characterizing the FT-IR spectrum of the raw materials, the FT-IR spectra of neat PUF prepared from castor oil was further analyzed. The FT-IR spectrum of the PUF revealed a broad absorption between 3250–2770 cm^{-1}, assigned mainly to N–H stretching of urethane groups, overlapped with residual O–H stretching. A distinct absorption at around 1535 cm^{-1} linked to amide II vibrations of the urethane structure. Additional peaks were observed at 670, 580, and 450 cm^{-1}, assigned to out-of-plane N–H bending and skeletal vibrations of the polyurethane backbone [36–38]. These features together confirm the successful formation of a urethane network from castor oil and diisocyanate precursors.

As shown in Figs. 3(d)–(h), the FT-IR spectra of silica-cellulose-filled PUF composites retained the general features of the neat PUF, however some differences are noticeable. A broad absorption band cantered at 2800–3180 cm^{-1} was present in all PUF composites. Compared with the neat PUF, this band appeared stronger, particularly in samples with higher filler loadings. No sharp free O–H peaks were detected in the region between 3600 and 3700 cm^{-1}, which indicated that hydroxyl groups were engaged in intermolecular interactions rather than existing in a free state. The amide II band at approximately 1535 cm^{-1} remains clear in all PUF composite samples, confirming that the polyurethane core structure in PUF composites is preserved [39,40]. In the fingerprint region, all PUF composite samples showed a clear absorption at 1020 cm^{-1}. This band can be attributed to overlapping C–O stretching vibrations from urethane linkages [41] and asymmetric Si–O–Si stretching from the silica component [42]. In addition, a band at around 800 cm^{-1} was found in all PUF composites. This peak, associated with Si–O rocking vibrations, was consistently detected across all loadings, which provides a clear spectral marker for silica incorporation into the PUF.

Generally, the FTIR results confirmed that the castor oil-based polyurethane and cellulose-silica filler could be successfully integrated. Although the main spectral properties were controlled by the PU matrix, the appearance of stronger hydrogen bond envelopes and the occurrence of silica-specific bands indicated that the filler contributed to the formation of the PUF chemical environment, which supported the improved interface compatibility and stability of the PUF compound. FTIR results confirmed the successful production of castor oil-based PUF and highlighted enhanced hydrogen bonding and filler-matrix interactions underlying the improved performance of cellulose-silica-reinforced PUF composites.

3.3. Thermal analysis

The thermogravimetric analysis (TGA) results (Figs. 4 and 5) demonstrate the influence of cellulose-silica additive concentration on the thermal stability of PUF composites. The characteristic degradation parameters, namely the onset of degradation (T_s), peak temperature (T_p), and end temperature (T_e), provide the degradation behavior of material.

From the heatmap (Fig. 4), it can be observed that neat PUF begins to degrade at T_s = 234.6°C, with T_p and T_e occurring at 328 and 435.9 °C, respectively. The incorporation of cellulose-silica additives alters these values in a concentration-dependent manner. At lower loadings (0.3–0.5 phr), T_s decreases slightly (e.g., 209.3 °C at 0.5 phr), suggesting a minor destabilizing effect at the early stage of degradation. However, with further increases in additive content (0.7–2.0 phr), T_s, T_p, and particularly T_e values shift toward higher temperatures. For example, the 0.7 phr formulation achieves the highest T_p (330 °C) and T_e (451.4 °C), while the 2.0 phr formulation maintains a T_e of 440.1 °C, both exceeding

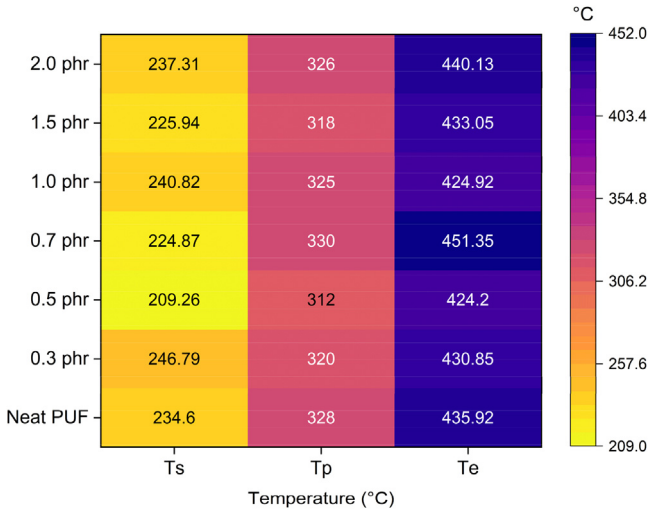

Fig. 4. Heatmap of thermogravimetric analysis (TGA) parameters for castor-oil-based PUFs with varying cellulose–silica additive concentrations. TGA was performed from 30 to 800 °C under a nitrogen atmosphere at a heating rate of 10 °C min^{-1}. The onset degradation temperature (T_s), peak degradation temperature (T_p, obtained from DTG maxima), and end degradation temperature (T_e) are presented. The shift of T_p and T_e toward higher temperatures, particularly at ≥0.7 phr, indicates enhanced thermal stability compared to neat PUF.

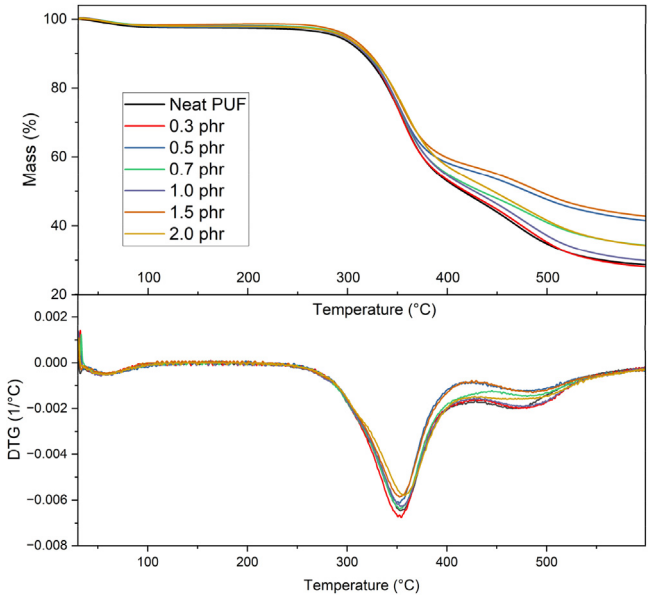

Fig. 5. (Top) Thermogravimetric (TGA) curves showing the percentage of mass remaining as a function of temperature. (Bottom) Derivative thermogravimetric (DTG) curves showing the rate of mass loss (dW/dT) as a function of temperature. Measurements were conducted from 30 to 800 °C under nitrogen at a heating rate of 10 °C min^{-1}. The addition of cellulose–silica decreases the maximum degradation rate and shifts the main degradation peaks to higher temperatures, confirming improved thermal resistance relative to neat PUF. Char yield was determined as the residual mass percentage at 800 °C under nitrogen.

that of neat PUF. This trend indicates that although small fluctuations in onset temperatures occur, the additives generally enhance thermal resistance, particularly in the later stages of decomposition.

The TGA and the derivative thermogravimetry (DTG) curves (Fig. 5) further illustrate these effects. Neat PUF exhibits a sharp mass loss around 326–330 °C, corresponding to rapid chain scission and volatilization of degradation products. In contrast, additive-containing samples

exhibit broader degradation profiles and lower mass-loss rates, as reflected in the DTG curves. The presence of additives reduces the maximum degradation rate while slightly shifting the decomposition peaks to higher temperatures. This suggests that the additives effectively alter the chemical environment within the polymer matrix, possibly by forming crosslinked networks or reinforcing structures that reduce the rate of degradation [43].

The enhancement in thermal resistance observed at 0.7 phr loading is closely linked to chemical interactions between the hybrid filler and the polyurethane matrix. FTIR analysis (Fig. 3) suggests that the hydroxyl groups (–OH) from the rice husk-derived cellulose and the silanol groups (Si–OH) on the silica surfaces facilitate new hydrogen bonding with the urethane N–H and C=O groups. These interactions effectively create a more robust cross-linked network that restricts the segmental mobility of the chains during thermal stress. During degradation, this filler network acts as a physical-chemical shield, slowing the diffusion of volatile fragments and promoting the formation of a stable, interconnected carbonaceous char. This mechanism directly explains the significantly higher char yield of 32% in the 50:50 hybrid baseline compared to the 25% yield of the neat matrix, confirming that the hybrid fillers serve as both structural reinforcement and thermal stabilizers.

Overall, these findings confirm that cellulose-silica additives improve the thermal stability of castor-oil-based polyurethane foams, particularly by delaying final degradation (T_e) and moderating degradation kinetics. Among the tested formulations, the 0.7 phr sample shows the most pronounced stabilization effect, while higher loadings (1.0–2.0 phr) also provide improvements compared to neat PUF. These results show that the optimized additive content for enhancing thermal stability exceeds 0.7 phr. While TGA effectively captures degradation behavior and filler-induced thermal stabilization, the present study did not directly resolve microphase separation or filler–matrix interfacial dynamics at the molecular scale. Due to the highly crosslinked and open-cell morphology of the foams, DSC transitions associated with glass transition were broad and difficult to interpret reliably. Therefore, TGA was prioritized to evaluate thermal stability relevant to acoustic applications. Future work will incorporate dynamic mechanical analysis (DMA) to more directly probe segmental mobility, microphase separation, and interfacial reinforcement mechanisms in this hybrid system.

3.4. Morphology and additive dispersion

Fig. 6 displays three sets of images captured using a mobile phone camera, an optical microscope (OM), and a scanning electron microscope (SEM) of the PUF loaded with cellulose-silica additives. Each set of images provides a significant view of the pore-size distribution, the dispersion of cellulose-silica additives within the PUF, the surface texture, and any potential agglomeration of the additives.

The mobile, OM, and SEM images (Fig. 6) provide a comprehensive view of the changes in pore structure and filler dispersion in polyurethane foam with varying concentrations of cellulose-silica additives. At lower filler concentrations (0.3, 0.5 phr), the foam retains a more open, uniform pore structure, with the additives well dispersed throughout the matrix, resulting in a consistent texture. As the filler concentration increases (0.7 to 2.0 phr), the texture becomes denser, and the pores shrink. Notably, at higher concentrations (1.0 phr and above), agglomeration of the additives becomes evident, with the fillers forming clusters that disrupt the uniformity of the pore structure, which is visible with a mobile phone camera presented in Fig. 6(a). The OM images in Fig. 6(b) confirm this, showing increasing irregularities in pore shape and size at higher concentrations. The SEM images in Fig. 6(c) provide a higher-magnification view, revealing that at lower concentrations, the pores remain smooth and evenly distributed, whereas at higher concentrations (1.5 and 2.0 phr), filler agglomeration is more pronounced, distorting the pore structure. This agglomeration may create localized areas of higher density, potentially affecting the mechanical properties of foams.

The cell size distribution (CSD) analysis (Fig. 7) further supports the SEM findings by quantitatively confirming the reduction in pore size with increasing additive content. For neat PUF, the distribution is broader with a higher mean pore diameter (0.347 mm), consistent with the relatively open-cell structure observed in SEM images. At low filler levels (0.3–0.7 phr), the CSD curves shift toward smaller pore diameters, with the mean values decreasing to 0.308 mm (0.3 phr), 0.204 mm (0.5 phr), and 0.203 mm (0.7 phr), indicating a more refined and uniform cell morphology. This trend aligns with the SEM images, which reveal more compact, evenly dispersed pores at these concentrations.

As the filler content exceeds 1.0 phr, the CSD broadens again, and the mean cell size increases (0.237–0.278 mm), suggesting reduced unifor-

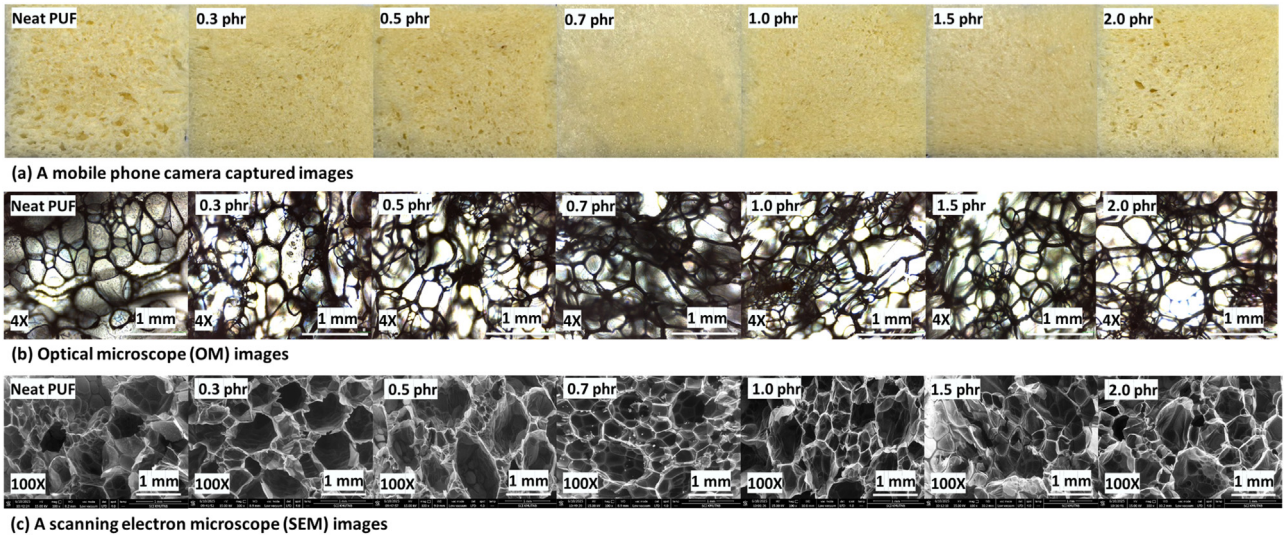

Fig. 6. Pore structure and additive dispersion in polyurethane foam at varying cellulose-silica concentrations: (a) Mobile images showing the overall foam texture at different filler levels (0.3 to 2.0 phr), (b) Optical microscope (OM) images with the objective's magnification 4x illustrating the pore distribution and irregularities by increasing additive concentration and (c) SEM images providing detailed views of the pore structure, highlighting the dispersion of additives and agglomeration at higher concentrations (1.5 and 2.0 phr). At lower concentrations, the foam exhibits a uniform, open pore structure, while at higher concentrations, noticeable filler agglomeration and pore distortion occur.

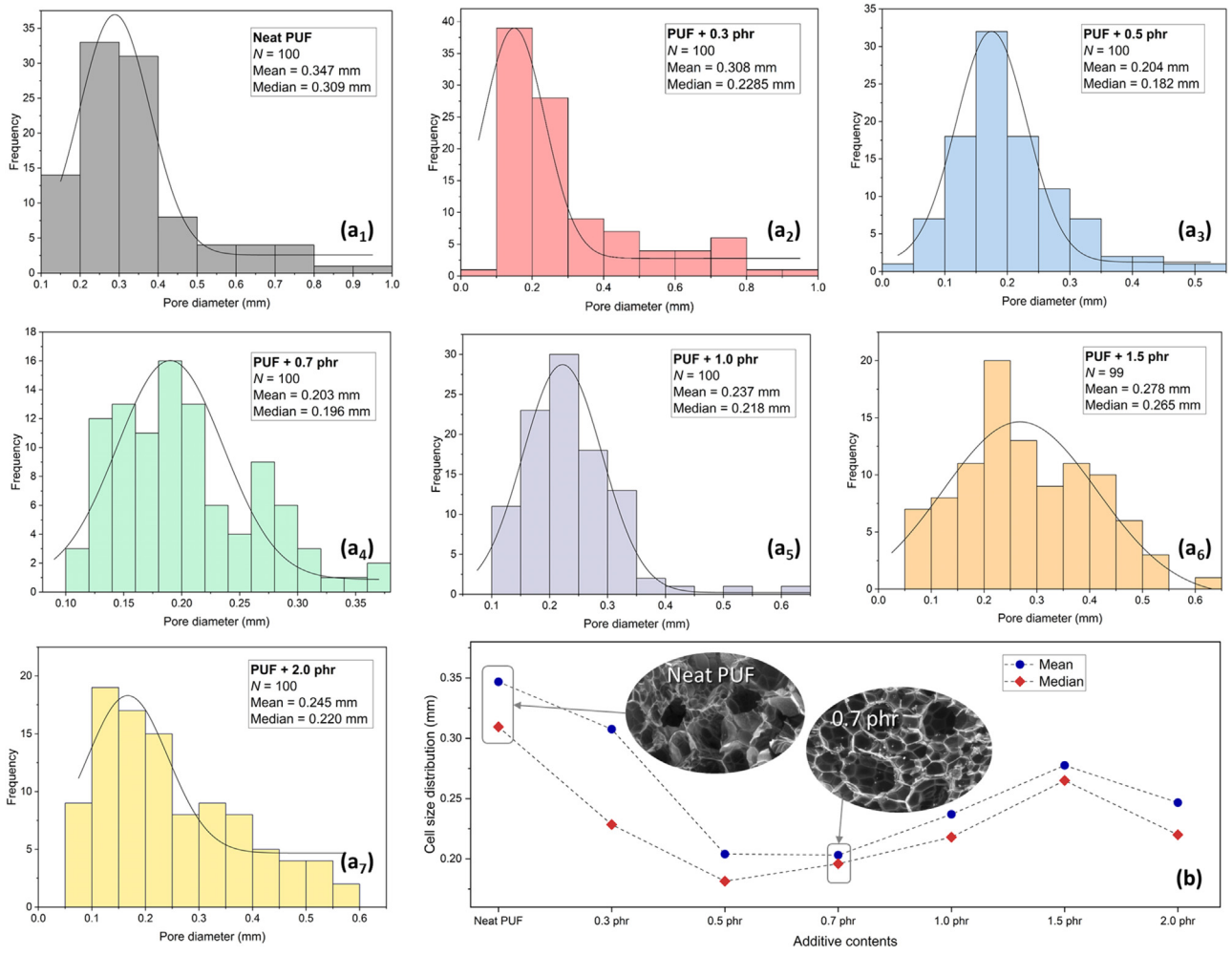

Fig. 7. Cell size distribution (CSD) histograms of (a_1–a_7) neat PUF and PUFs with varying filler concentrations (0.3–2.0 phr), along with (b) the mean and median values plotted against filler content. Neat PU exhibits a broad distribution with larger mean pore diameters, consistent with the open-cell morphology observed in SEM images. At low filler concentrations (0.3–0.7 phr), the distributions shift toward smaller and more uniform pore sizes, confirming the refined cell structure seen in SEM, Fig. 6. With higher filler loadings (≥1.0 phr), the distributions broaden again and shift toward larger pores, indicating reduced uniformity and possible agglomeration, in agreement with the SEM observations of disrupted pore morphology.

mity and possible agglomeration. Particularly at 1.5 phr and 2.0 phr, the shift toward larger cell sizes with wider distributions corresponds with the SEM evidence of disrupted pore uniformity and localized clustering of additives. Thus, the CSD data not only confirms the morphological transition observed in SEM but also highlights the optimal filler concentration (around 0.5–0.7 phr) where the pore structure achieves the most uniform refinement.

3.5. *Mechanical performance*

Fig. 8 illustrates the stress–strain behavior of neat PUF and PUF composites containing different filler loadings. Neat PUF exhibits a relatively low stress response with an almost linear increase in stress as strain increases, indicating a compliant and less reinforced structure. In contrast, the filled systems show a pronounced enhancement in stress response over the entire strain range, with stress rising more rapidly with strain compared to neat PUF. As filler content increases, the curves shift progressively upward, reflecting improved stiffness and load-bearing capacity. The composites display a nonlinear stress–strain profile, particularly at lower strains (0–5% strain), indicating an initial reinforcement effect where the filler restricts polymer chain mobility and efficiently transfers stress from the matrix to the filler. At higher deformation (above 5% strain), polymer chains progressively align and stretch, while sus-

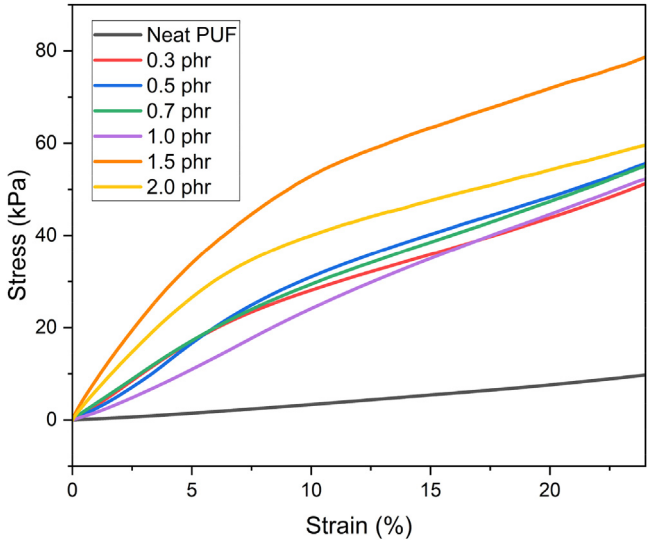

Fig. 8. Stress–strain curves of neat PUF and PUF composites with varying filler loadings, illustrating the influence of filler incorporation on the deformation behavior under tensile loading.

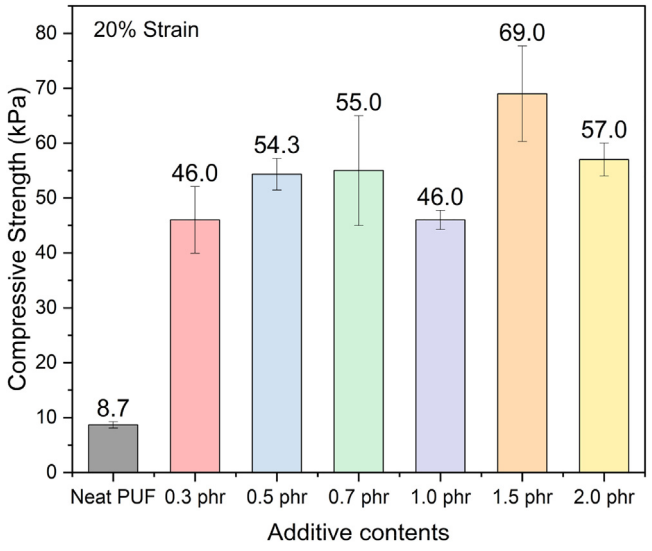

Fig. 9. Compressive strength of PU foams with varying cellulose/silica additive contents at 20% strain.

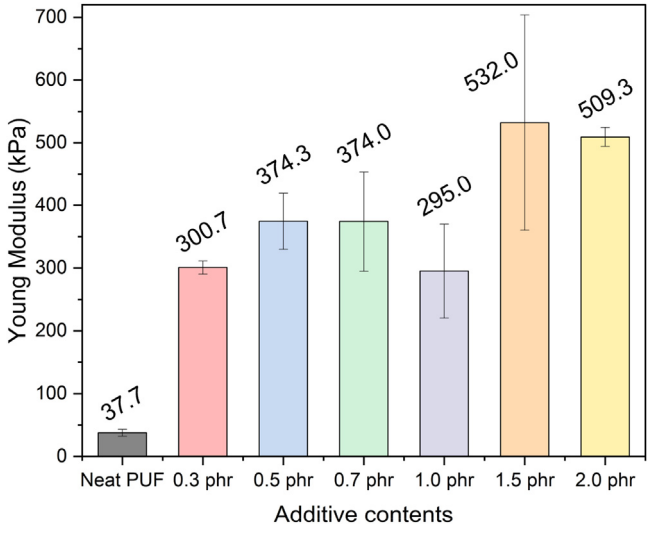

Fig. 10. Young's modulus of PU foams with different cellulose/silica additive contents.

tained filler–matrix interactions continue to resist deformation, leading to a steady increase in stress rather than sudden failure. Overall, the presence and increasing amount of filler significantly modify the deformation behavior of PUF, resulting in stronger resistance to applied strain and a more robust mechanical response, thereby complementing the Young's modulus data and compressive strength presented in Figs. 9 and 10, respectively.

The compressive behavior of the PUF composites (Fig. 9) shows a clear dependence on additive content. At 20% strain, the neat PUF displays the lowest compressive strength (8.7 kPa), reflecting its inherently weak cellular structure. With the addition of small amounts of additive (0.3–0.7 phr), the compressive strength increases significantly to 46.0–55.0 kPa. This improvement suggests that the additive effectively reinforces the foam skeleton, enhances stress transfer, and stabilizes the cell walls. However, at 1.0 phr, a drop in compressive strength (46.0 kPa) is observed, which indicates poor dispersion or localized agglomeration of the additives, leading to stress concentration points within the foam [44]. The maximum compressive strength is reached at 1.5 phr (69.0 kPa), after which a slight reduction is noted at 2.0 phr (57.0 kPa). This indicates that excessive loading no longer contributes to reinforcement and may instead hinder uniform stress distribution within the foam structure.

Young's modulus, which reflects the stiffness of the foams, follows a similar trend presented in Fig. 10. Neat PUF exhibits the lowest modulus (37.7 kPa), while additive incorporation substantially enhances stiffness, particularly at 0.3–0.7 phr (300.7–374.3 kPa). A slight decrease occurs at 1.0 phr (295.0 kPa), again consistent with structural imperfections induced by poor dispersion. The highest stiffness is observed at 1.5 phr (532.0 kPa), confirming that this concentration yields the most rigid structure. At 2.0 phr, the modulus remains elevated (509.3 kPa) but does not surpass the 1.5 phr sample.

Together, these results highlight a balance between stiffness and resilience. Additive incorporation markedly improves both compressive strength and stiffness compared to neat PUF, but excessive loading beyond the optimum (1.5 phr) leads to diminished performance. Although the compressive and modulus results suggest higher stiffness at higher additive loadings, this rigidity is not ideal for practical applications that require sound absorption and resilience. Considering compressive strength, stiffness, cell-size distribution, and thermal stability, the PUF with 0.7 phr additive emerges as the most balanced formulation. At this composition, the foam provides sufficient strength (≈55 kPa) and stiffness (≈374 kPa) for structural stability, while maintaining deformability for effective acoustic damping. The favorable cell morphology and improved thermal stability further support its suitability, and as shown in the acoustic properties section, the sound absorption performance of the 0.7 phr sample aligns well with this conclusion.

Single-filler systems with high effectiveness often lead to processing challenges or brittleness. The 50:50 ratio was chosen to exploit the hierarchical network, in which silica prevents cellulose bundling—a mechanism supported by Karger-Kocsis et al. (2014) and Swolfs et al. (2016) [45,46]—to ensure a more uniform internal architecture. By fixing the ratio, the study isolates the impact of total filler content on the structural and thermal evolution of composites. Preliminary comparison with pure-filler counterparts (see Table 1) confirms that this hybrid ratio yields a balanced material with significant mechanical reinforcement over the neat matrix and enhanced thermal durability compared to individual components.

As demonstrated in Table 1 and the expanded discussion, the 50:50 ratio was chosen to prioritize a balance of properties—maximizing thermal stability via char yield while maintaining a 532% increase in modulus over the neat matrix—providing a robust platform for the content-dependency analysis that is the focus of this work.

3.6. Moisture absorption

The short-term absorption profiles (Fig. 11(a)) show that all PUF samples undergo rapid moisture uptake during the first 85 min, after which most formulations approach equilibrium. However, samples with low additive contents (0.3 and 0.5 phr) continue to show a slight increase even at 300 min, indicating a slower stabilization process compared to higher loadings. By contrast, the other formulations reach

Table 1
Comparative analysis of mechanical and thermal properties of neat PUF, single-filler controls, and the hybrid formulation at a representative total filler loading of 0.7 phr. Compressive strength was measured at 20% strain. Char yield corresponds to the residual mass percentage at 800 °C determined by TGA under nitrogen (30–800 °C, 10 °C min^{-1}).

Samples	Ratio (Cel:Sil)	Compressive Strength @20% strain	Char Yield at 800 °C
Neat Matrix	0:0	8.7 ± 0.6 kPa	~ 25%
Pure Cellulose	100:0	57.7 ± 4.9 kPa	~ 25%
Pure Silica	0:100	72.7 ± 9.5 kPa	~ 27%
Hybrid (50:50)	**50:50**	**55.0 ± 10 kPa**	**~ 32%**

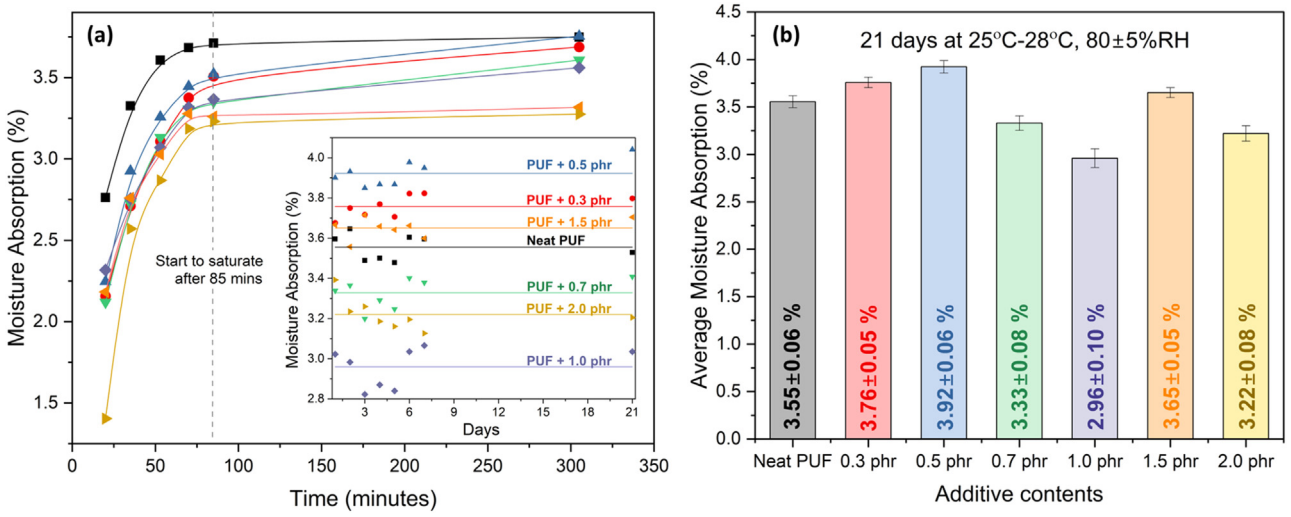

Fig. 11. Moisture absorption of neat PUF and additive-modified PUFs under 80 ± 5% relative humidity at room temperature. (a) Short-term absorption profiles showing rapid uptake during the first 85 min, followed by equilibrium (inset, 21 days). Neat PUF exhibits the highest absorption rate in short-term, whereas additive-modified foams show reduced uptake. (b) Long-term absorption after 21 days confirms that formulations with ≥0.7 phr additive maintain lower equilibrium values, with 1.0 phr demonstrating the most effective resistance.

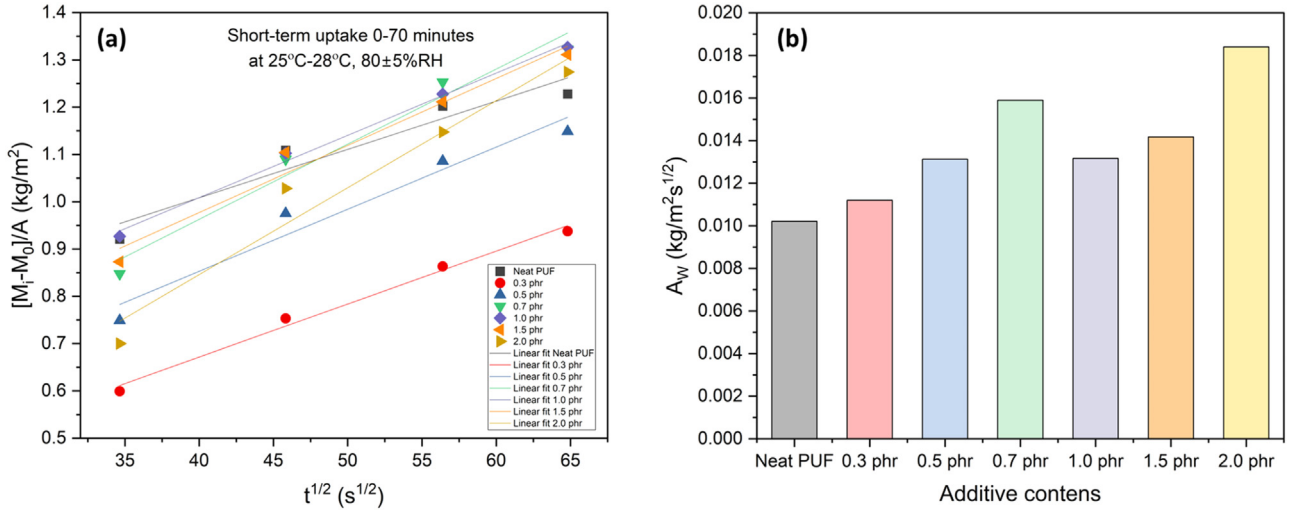

Fig. 12. (a) Linear fitting of short-term water uptake (0–70 min) for neat PUF and additive-modified foams at 25–28 °C and 80 ± 5% relative humidity, used to calculate the absorption coefficient A_W. (b) Water absorption coefficient (A_W) values for different additive contents, showing higher initial uptake rates at 0.7 and 2.0 phr.

steady absorption levels more quickly. After one full day, all samples display steady absorption rates, suggesting that equilibrium is reached within this timeframe. The long-term data (inset of Figs. 11(a)(b)) provide further confirmation. After 21 days at 25–28 °C and 80 ± 5% relative humidity, neat PUF exhibited an average absorption of 3.55 ± 0.06%. In comparison, PUF with 1.0 phr achieved the lowest value (2.96 ± 0.10%), followed by 2.0 phr (3.22 ± 0.08%) and 0.7 phr (3.33 ± 0.08%). These formulations clearly outperform neat PUF and other loadings, demonstrating that the additive effectively reduces water uptake and enhances dimensional stability.

The moisture absorption behavior exhibits a nonlinear trend, where low additive contents (0.3 and 0.5 phr) not only failed to improve absorption but also resulted in values higher than those of neat PUF (3.76 ± 0.05% and 3.92 ± 0.06%, respectively). This behavior suggests that insufficient additive levels are ineffective at altering the polymer matrix and may promote localized heterogeneities—such as interfacial microvoids—that serve as preferential sites for water ingress [47]. At these low contents, the fillers likely act as moisture traps rather than a cohesive barrier network. However, at concentrations of 0.7 phr or higher, a critical threshold is reached at which pore refinement and improved interfacial bonding effectively seal these pathways. FTIR analysis (Fig. 3) supports this transition, indicating enhanced hydrogen bonding between the silica/cellulose hydroxyl groups and the urethane matrix, which mitigates moisture ingress. Overall, the results suggest that additive concentrations above 0.7 phr optimize moisture resistance, with 1.0 phr emerging as the most effective formulation for long-term durability in humid environments.

The water absorption coefficient (A_W) calculated from the linear uptake region is presented in Fig. 12. This coefficient represents the initial rate of moisture ingress, which depends on both the exposure time and the cross-sectional area of specimens, as expressed in Eq. (1). Among the modified foams, the 0.7 phr and 2.0 phr samples exhibited relatively high A_W values, indicating a faster short-term uptake compared to the other formulations. However, the long-term equilibrium moisture absorption data (Fig. 11(b)) show a different trend. Despite their higher A_W, the 0.7 and 2.0 phr samples stabilized at significantly lower mois-

ture content after 21 days, together with the 1.0 phr sample. In contrast, low additive contents (0.3 and 0.5 phr) not only absorbed moisture at a slower initial rate but also exhibited higher equilibrium values than neat PUF, confirming their limited effectiveness. This suggests that while higher additive levels may facilitate rapid initial surface penetration, they ultimately restrict long-term moisture retention within the foam structure.

The apparent divergence between short-term absorption rate (A_W^S) and long-term equilibrium uptake reflects multi-stage moisture transport behavior in open-cell foams. During the early stage, absorption is dominated by surface wetting and capillary penetration into accessible pore channels, which may produce relatively high A_W^S values even when equilibrium retention remains limited. In contrast, long-term uptake is governed by pore connectivity, diffusion resistance, and effective free volume. At ≥0.7 phr, refined cell walls and partial pore obstruction reduce continuous diffusion pathways, thereby restricting equilibrium moisture accumulation despite initial surface wetting effects. While contact angle analysis and mercury intrusion porosimetry were not conducted in the present study, these techniques will be incorporated in future work to quantitatively validate interfacial wettability and pore-network evolution and to further substantiate the proposed mechanism.

The SEM images (Fig. 6) help explain these observations. At low filler contents (0.3 and 0.5 phr), the pore morphology remains open and interconnected, providing pathways that facilitate long-term moisture diffusion and storage. As the filler concentration increases, particularly above 0.7 phr, the pores become more compact and irregular. This compact cellular architecture may initially allow quicker surface penetration but reduces overall pore connectivity and free volume, thereby limiting the equilibrium moisture uptake. Taken together, these results indicate that additive concentrations above 0.7 phr optimize moisture resistance in PUF. Although the short-term absorption coefficient is relatively high at 0.7 and 2.0 phr, the compact structure achieved at higher filler contents effectively limits long-term water retention, with 1.0 phr providing the best balance between initial absorption behavior and final stability.

The results suggest that the increased filler content enhances the resistance of foams to moisture penetration by modifying their microstructure and reducing porosity. The SEM images complement the moisture absorption analysis by showing the structural transitions in the material, with denser structures potentially leading to reduced moisture uptake. This relationship highlights the crucial role of filler composition and porosity in controlling the moisture resistance of materials.

3.7. Acoustic properties

The sound absorption spectra of 7 formulas including neat PUF and PUF filled with a 50:50 silica–cellulose mixture (0.3, 0.5, 0.7, 1.0, 1.5 and 2.0 phr) were averaged from three replicate measurements after interpolation onto a common frequency axis (200–5000 Hz) presented in Fig. 13(a). The averaged curves highlight how filler addition influences absorption performance across the low, middle, and high frequency regions. At low frequencies (200–500 Hz), all formulations exhibited sound absorption coefficients (SAC) below the practical threshold of 0.40, reflecting the typical limitations of 4-cm foams at long wavelengths. In the mid-frequency region (500–2000 Hz), neat PUF maintained broad absorption around and above the 0.40 threshold, while the 0.7 phr formulation tracked most closely, preserving mid-band absorption capacity. By contrast, the 0.3 and 0.5 phr samples remained largely below 0.40, and the 2.0 phr sample showed a marked reduction across the band. At higher frequencies (2000–5000 Hz), neat PUF again exceeded 0.5, whereas most filled systems, particularly 2.0 phr, failed to reach similar levels. Overall, neat PUF provided the most balanced broadband absorption, while 0.7 phr was the only filled system to approximate its performance.

To quantify mid-band absorption, the Noise Reduction Coefficient (NRC) was calculated as the mean SAC at 250, 500, 1000, and 2000 Hz presented in Fig. 13(b). Neat PUF showed an NRC of 0.422 ± 0.083, whereas filler-modified foams varied between 0.153 and 0.364. Statistical comparison using Welch's t-test confirmed that 0.3, 0.5, and 2.0 phr were significantly lower than neat PUF ($p < 0.05$), while 0.7 phr, 1.0, and 1.5 phr were not significantly different. These findings indicate that light or heavy filler additions reduce mid-band absorption, with only the moderate 0.7 phr formulation preserving NRC close to neat PUF.

Because NRC considers only four frequency points, the Sound Absorption Average (SAA) was also evaluated and shown in Fig. 13(b). Here, SAC values were averaged across 1/3-octave band centers from 200 to 4000 Hz, providing a broader view of mid- to high-frequency absorption. Neat PUF recorded an SAA of 0.489 ± 0.069, while filled foams ranged between 0.213 and 0.450. T-tests showed that 0.3 phr, 0.5, 1.0, and 2.0 phr were significantly lower than neat PU ($p < 0.05$). In contrast, 0.7 phr again showed no significant difference, and 1.5 phr trended lower ($p \approx 0.06$) but did not reach statistical significance. This broader frequency integration revealed that even the 1.0 phr foam, not detected by NRC, suffered a meaningful reduction when higher mid-frequencies were included.

Comparing NRC and SAA demonstrates the importance of using both indices. NRC is a useful and widely recognized single-number rating, but it may underestimate differences that emerge when a broader frequency band is considered. SAA, by integrating across 200–4000 Hz, proved more sensitive to spectral changes, particularly in identifying the reduced performance of the 1.0 phr foam. Together, the two metrics show a consistent underperformance of 0.3, 0.5, and 2.0 phr samples, while 0.7 phr consistently matches neat PUF across both metrics. These results suggest that moderate filler addition at 0.7 phr can retain acoustic functionality, while lighter or heavier loadings compromise broadband sound absorption.

The sound absorption performance of the developed castor oil–based PUF composites was benchmarked against a commercial low-density petroleum-based PU foam (≈0.09 g cm^{-3}) commonly used for acoustic applications presented in Fig. 13. The commercial foam exhibits an SAA of 0.470 ± 0.010, which is comparable to that of the neat castor oil–based PUF (0.489 ± 0.069). Despite similar acoustic performance, the neat castor oil PUF demonstrates a substantially higher compressive modulus (~38 kPa) than the commercial foam (~25 kPa), indicating enhanced mechanical robustness without sacrificing sound absorption. Moreover, the hybrid foam containing 0.7 phr rice husk–derived silica and cellulose, which exhibits the best mechanical performance among all formulations, achieves an SAA comparable to the commercial foam. This result demonstrates that effective sound absorption can be retained even with increased stiffness, despite the relatively more closed-cell structure of castor oil–based PUFs, due to enhanced interfacial damping and energy dissipation introduced by bio-derived fillers. In addition to competitive performance, the use of renewable castor oil and agricultural waste–derived fillers significantly reduces reliance on petroleum-based materials, highlighting the strong potential of these bio-based PUFs as sustainable alternatives for acoustic applications that require both mechanical durability and environmental responsibility.

The 0.7 phr formulation provides the best acoustic-to-mechanical ratio, ensuring maximum sound mitigation while maintaining thermal and moisture integrity. The decision to prioritize the 0.7 phr formulation is supported by the work of Tiuc et al. (2016) and Kairytė, A., et al. (2018) [48,49], who demonstrated that excessive filler loading in PU foams can lead to cell wall thickening and reduced acoustic attenuation while preserving the insulating and lightweight properties of the foam. Furthermore, the processing advantages of lower viscosity in bio-polyol systems reported by Shaik et al. (2024) [50] confirm that 0.7 phr allows for a more homogeneous cell distribution than the 1.5 phr variant. As detailed in Table 2, while the 1.5 phr formulation yields the highest compressive strength, a comprehensive trade-off analysis indicates that the 0.7 phr loading provides a more balanced profile, maintaining significant mechanical reinforcement without compromising the acoustic functionality of the biocomposite.

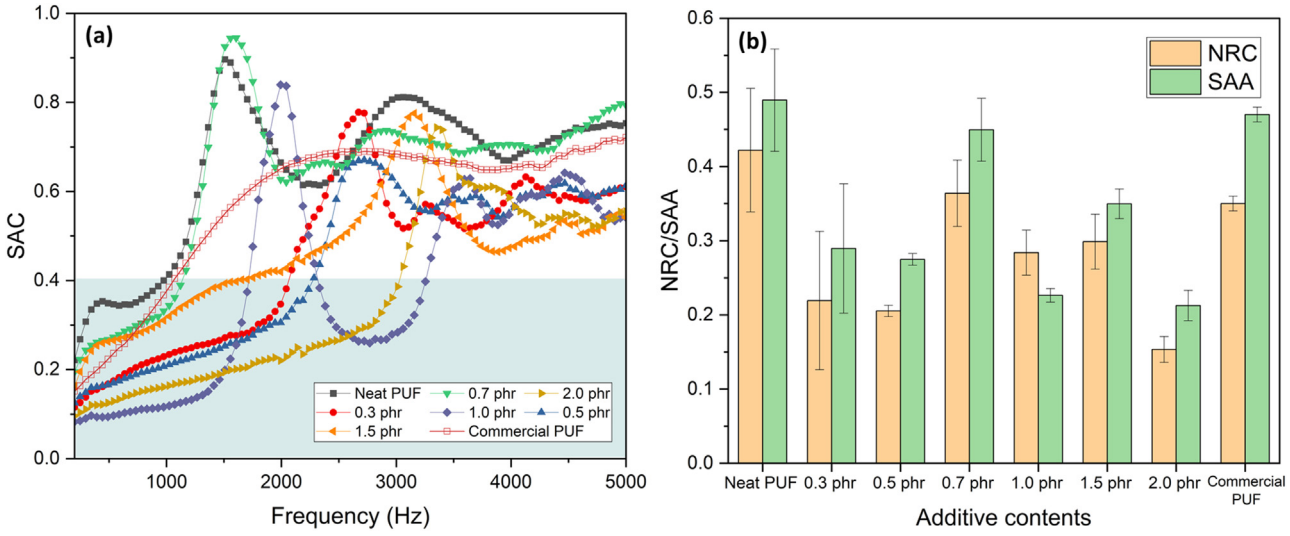

Fig. 13. (a) Normal-incidence sound absorption coefficient (SAC) spectra of neat PUF and PUF composites with varying silica–cellulose additive contents (0.3–2.0 phr) and a commercial PUF. (b) Comparison of noise reduction coefficient (NRC) and sound absorption average (SAA) values derived from the SAC spectra.

Table 2
Multi-criteria performance and cost-benefit analysis of castor oil-based PU foam composites at varying filler loadings. The comparison highlights the trade-offs between mechanical reinforcement, thermal stability, moisture resistance, and acoustic efficiency, identifying 0.7 phr as the optimal formulation for high-performance acoustic applications.

Property		0.7 phr (Balanced)	1.5 phr (Max Strength)	Impact of Higher Loading (above 1.5 phr)
Compressive Strength		~ 58.0 kPa	~ 69.0 kPa	+19% Improvement
Thermal stability	T_p	330 °C	318 °C	Lower peak degradation resistance.
	T_e	451 °C	433 °C	18.3 °C reduction in final stability.
Moisture Absorption	Long-term (21d)	3.33%	3.65%	Increased susceptibility to humidity.
	Short-term Uptake Rate	Moderate	High	Faster initial water penetration.
Acoustic Property	Peak SAC	~ 0.95	~0.78	18% reduction in peak absorption.
	Profile	Superior mid-freq (~1500 Hz)	Shifted to high-freq (~3200 Hz)	Narrower application range.
	NRC/SAA	0.36/0.45	0.30/0.35	Reduce mid-band absorption
Processing		Low/Manageable	High	Harder to process
Cost/Resource Use		Baseline	>2x Filler usage	Increased material cost

In summary, Table 2 provides a comparative evaluation of all studied properties, concluding that the 0.7 phr formulation represents the optimal trade-off between peak sound absorption, thermal stability, moisture resistance, and mechanical performance.

4. Conclusion

This study successfully synthesized bio-based polyurethane foams using castor oil as a renewable polyol and reinforced them with rice husk-derived silica and cellulose. The resulting foams demonstrated clear improvements in physical and acoustic properties compared to neat PUF, confirming the effectiveness of the additive strategy. Mechanical testing showed enhanced compressive strength and stiffness at optimal loadings, while acoustic evaluations indicated that moderate filler levels preserved sound absorption performance. Thermal analysis further confirmed improved stability, and moisture uptake studies highlighted reduced water absorption at higher filler contents.

These findings demonstrate that sustainable sourcing and functional performance can be achieved simultaneously, indicating the potential of these materials as alternatives to petroleum-derived foams for acoustic and structural applications. In conclusion, this study establishes the foundational properties of the 50:50 cellulose/silica hybrid system, highlighting the total filler content as a primary driver of composite performance. To further advance the sustainability of these green foams, future research will investigate the incorporation of bio-based or less-toxic isocyanate components to replace traditional petroleum-derived precursors. Additionally, research is underway to optimize the silica-to-cellulose ratio, which is expected to provide finer control over pore morphology and mechanical stiffness. Subsequent phases of this work will evaluate flammability, antimicrobial performance, and aging resistance—specifically through UV exposure and fatigue testing via long-term mechanical cycling—to simulate the harsh environmental conditions of Southeast Asia. While the present study verifies the fundamental multifunctional performance of the hybrid system under controlled laboratory conditions, comprehensive long-term durability and environmental stability assessments are required before large-scale or industrial implementation can be fully validated.

Decleration of Competing Interest

The authors declare that they have no known competing financial interests or personal relationships that could have appeared to influence the work reported in this paper.

CRediT authorship contribution statement

Nathapong Sukhawipat: Writing – original draft, Supervision, Methodology, Investigation, Formal analysis, Conceptualization. **Thitaree Phokasem:** Methodology, Investigation, Formal analysis, Data curation. **Nutcha Sukkun:** Methodology, Investigation, Formal analysis, Data curation. **Purintorn Chanlert:** Writing – original draft, Supervision, Methodology, Formal analysis, Conceptualization. **Wichain Chailad:** Writing – original draft, Supervision, Formal analysis, Data curation, Conceptualization. **Narongrit Sosa:** Writing – original draft,

Supervision, Methodology, Investigation, Conceptualization. **Ziyin Xiang:** Supervision, Conceptualization. **Arreerat Jiamprasertboon:** Supervision, Conceptualization. **Kritsadi Thetpraphi:** Writing – original draft, Validation, Supervision, Resources, Project administration, Funding acquisition, Formal analysis, Data curation, Conceptualization.

Acknowledgements

This research was funded by the New Researcher Development program (contract number WU69204). Moreover, we would like to thank the Interfaculty Collaboration Senior Project Award 2025 from King Mongkut's University of Technology North Bangkok, Thailand.

Supplementary materials

Supplementary material associated with this article can be found, in the online version, at doi:10.1016/j.chphma.2026.03.007.

References

[1] E. Martwong, T. Yingshataporn-a-nan, T. Minanandana, K. Puksuwan, J. Junthip, N. Sukhawipat, Sound absorption and thermal insulation materials from waste palm oil for housing application: Green polyurethane/water hyacinth fiber sheet composite, Constr. Build. Mater. 438 (2024) 137007, doi:10.1016/j.conbuildmat.2024.137007.
[2] N. Sukhawipat, T. Yingshataporn-A-Nan, T. Minanandana, K. Puksuwan, L. Saengdee, Y. Nakaramontri, N. Sosa, N. Saetung, Effects of water hyacinth fiber size on sound absorption properties of advanced recycled palm oil-based polyurethane foam composite„ Mater. Today Proc. 52 (2021) 2409–2413, doi:10.1016/j.matpr.2021.10.417.
[3] N. Sukhawipat, L. Saengdee, P. Pasetto, J. Junthip, E. Martwong, Sustainable rigid polyurethane foam from wasted palm oil and water hyacinth fiber composite—A green sound-absorbing material, Polymers 14 (2022) 201, doi:10.3390/polym14010201.
[4] M. Szpiłyk, R. Lubczak, J. Lubczak, The biodegradable cellulose-derived polyol and polyurethane foam, Polym. Test. 100 (2021) 107250, doi:10.1016/j.polymertesting.2021.107250.
[5] A. Das, P. Mahanwar, A brief discussion on advances in polyurethane applications, Adv. Ind. Eng. Polym. Res. 3 (2020) 93–101, doi:10.1016/j.aiepr.2020.07.002.
[6] T. Kattiyaboot, C. Thongpin, Effect of natural oil based polyols on the properties of flexible polyurethane foams blown by distilled water, Energy Procedia 89 (2016) 177–185, doi:10.1016/j.egypro.2016.05.024.
[7] N.E. Marcovich, M. Kurańska, A. Prociak, E. Malewska, K. Kulpa, Open cell semi-rigid polyurethane foams synthesized using palm oil-based bio-polyol, Ind. Crops Prod. 102 (2017) 88–96, doi:10.1016/j.indcrop.2017.03.025.
[8] L. Yuvaraj, S. Jeyanthi, M.L. Babu, Sound absorption analysis of castor oil based polyurethane foam with natural fiber„ Mater. Today Proc. 5 (2018) 23534–23540, doi:10.1016/j.matpr.2018.10.141.
[9] R.H. Patel, M.D. Shah, H.B. Patel, Synthesis and characterization of structurally modified polyurethanes based on castor oil and phosphorus-containing polyol for flame-retardant coatings, Int. J. Polym. Anal. Charact. 16 (2011) 107–117, doi:10.1080/1023666X.2011.541108.
[10] D. Riyapan, A. Saetung, N. Saetung, A novel rigid PU foam based on modified used palm oil as sound absorbing material, J. Polym. Environ. 27 (2019) 1693–1708, doi:10.1007/s10924-019-01460-9.
[11] A.H. Shaik, S. Banerjee, A. Rahaman, S. Agashe, A. Khan, M.R. Chandan, One-step synthesis and characteristics of LiOH-castor oil based stable polyurethane foam, J. Polym. Res. 28 (2021) 220, doi:10.1007/s10965-021-02580-4.
[12] A. Hussain Shaik, R. Jain, S. Manchikanti, K. Krishnamoorthy, D. Kumar Bal, A. Rahaman, S. Agashe, M.Rehaan Chandan, Reinstating structural stability of castor oil based flexible polyurethane foam using glycerol, ChemistrySelect 5 (2020) 3959–3964, doi:10.1002/slct.202000784.
[13] G. Sung, J.H. Kim, Effect of high molecular weight isocyanate contents on manufacturing polyurethane foams for improved sound absorption coefficient, Korean J. Chem. Eng. 34 (2017) 1222–1228, doi:10.1007/s11814-016-0361-6.
[14] F. Coccia, L. Gryshchuk, P. Moimare, F.D. Bossa, C. Santillo, E. Barak-Kulbak, L. Verdolotti, L. Boggioni, G.C. Lama, Chemically functionalized cellulose nanocrystals as reactive filler in bio-based polyurethane foams, Polymers 13 (2021) 2556, doi:10.3390/polym13152556.
[15] D.I. Lee, Y.H. Ha, H. Jeon, S.H. Kim, Preparation and properties of polyurethane composite foams with silica-based fillers, Appl. Sci. 12 (2022) 7418, doi:10.3390/app12157418.
[16] B. Merillas, A. Lamy-Mendes, F. Villafañe, L. Durães, M.Á. Rodríguez-Pérez, Polyurethane foam scaffold for silica aerogels: Effect of cell size on the mechanical properties and thermal insulation, Mater. Today Chem. 26 (2022) 101257, doi:10.1016/j.mtchem.2022.101257.
[17] M. Imran, A. Rahaman, A.H. Shaik, M.R. Chandan, Stability enhancement of highly loaded nano-clay-based flexible polyurethane foams using hollow glass microspheres, J. Cell. Plast. 56 (2020) 547–557, doi:10.1177/0021955X20912203.
[18] C.V. Vinay, D.M. Varma, M.R. Chandan, P. Sivabalan, A.K. Jaiswal, S. Swetha, A. Sionkowska, B. Kaczmarek, Study of castor oil-based auxetic polyurethane foams for cushioning applications, Polym. Int. 70 (2021) 1631–1639, doi:10.1002/pi.6259.
[19] A.A. Maamoun, A. Elkhateeb, S. Zulfiqar, Halloysite-decorated mechanically robust polyurethane nanocomposite foams for acoustic relevance, Ind. Eng. Chem. Res. 61 (2022) 17937–17949, doi:10.1021/acs.iecr.2c03535.
[20] N. Sukhawipat, T. Kongprabat, N. Uthaipan, A. Saetung, N. Saetung, A new green rigid polyurethane foam based on modified palm oil: Preliminary study of their potential for marine buoy applications, J. Appl. Polym. Sci. 142 (2025) e56477, doi:10.1002/app.56477.
[21] N. Sukhawipat, Modified used palm oil polyols–A new waste-based plasticizer for thermoplastic non-glutinous starch foam, 2022, doi:10.21203/rs.3.rs-2037290/v1.
[22] S. Limrungruengrat, N. Sosa, J. Jitcharoen, T. Chotchuangchutchaval, N. Sukhawipat, Polybutylene succinate/calcium carbonate based biocomposite film reinforced with silica derived from non-glutinous rice husk, J. Polym. Environ. 31 (2023) 5401–5415, doi:10.1007/s10924-023-02965-0.
[23] W. Kliengchuay, R. Mingkhwan, N. Kiangkoo, S. Suwanmanee, N. Sahanavin, J. Kongpran, H.W. Aung, K. Tantrakarnapa, Analyzing temperature, humidity, and precipitation trends in six regions of Thailand using innovative trend analysis, Sci. Rep. 14 (2024) 7800, doi:10.1038/s41598-024-57980-5.
[24] M. Bomberg, M. Pazera, R. Plagge, Analysis of selected water absorption coefficient measurements, J. Therm. Envel. Build. Sci. 28 (2005) 227–243, doi:10.1177/1097196305047003.
[25] P. Chanlert, S. Tongyoo, C. Rordrak, Effects of urea–formaldehyde and polyvinyl acetate adhesive on sound absorption coefficient and sound transmission loss of palmyra palm fruit fiber composites, Appl. Acoust. 198 (2022) 108984, doi:10.1016/j.apacoust.2022.108984.
[26] P. Chanlert, A. Jintara, W. Manoma, Comparison of the sound absorption properties of acoustic absorbers made from used copy paper and corrugated board, Bioresources 17 (2022) 5612, doi:10.15376/biores.17.4.5612-5621.
[27] R. Ledesma-Amaro, J.M. Nicaud, Yarrowia lipolytica as a biotechnological chassis to produce usual and unusual fatty acids, Prog. Lipid Res. 61 (2016) 40–50, doi:10.1016/j.plipres.2015.12.001.
[28] H.M. Fahmy, A. Amr, Synthesis of castor oil/PEG as textile softener, Sci. Rep. 14 (2024) 7208, doi:10.1038/s41598-024-56917-2.
[29] H. Li, S. Niu, C. Lu, Pyrolysis characteristics of castor oil through thermogravimetric coupled with fourier transform infrared spectroscopy, Procedia Eng 205 (2017) 3705–3710, doi:10.1016/j.proeng.2017.10.292.
[30] S.V. Araújo, B.S. Rocha, F.M.T. Luna, E.M. Rola, D.C.S. Azevedo, C.L. Cavalcante, FTIR assessment of the oxidation process of castor oil FAME submitted to PetroOXY and Rancimat methods, Fuel Process. Technol. 92 (2011) 1152–1155, doi:10.1016/j.fuproc.2010.12.026.
[31] S. Cichosz, A. Masek, K. Wolski, M. Zaborski, Universal approach of cellulose fibres chemical modification result analysis via commonly used techniques, Polym. Bull. 76 (2019) 2147–2162, doi:10.1007/s00289-018-2487-7.
[32] R. Vârban, I. Crișan, D. Vârban, A. Ona, L. Olar, A. Stoie, R. Ștefan, Comparative FT-IR prospecting for cellulose in stems of some fiber plants: Flax, velvet leaf, hemp and jute, Appl. Sci. 11 (2021) 8570, doi:10.3390/app11188570.
[33] I. Spiridon, C.A. Teacă, R. Bodîrlău, Structural changes evidenced by FTIR spectroscopy in cellulosic materials after pre-treatment with ionic liquid and enzymatic hydrolysis, BioResources 6 (2010) 400–413, doi:10.15376/biores.6.1.400-413.
[34] R.F.S. Lenza, W.L. Vasconcelos, Preparation of silica by sol-gel method using formamide, Mater. Res. 4 (2001) 189–194, doi:10.1590/S1516-14392001000300008.
[35] R. Ellerbrock, M. Stein, J. Schaller, Comparing amorphous silica, short-range-ordered silicates and silicic acid species by FTIR, Sci. Rep. 12 (2022) 11708, doi:10.1038/s41598-022-15882-4.
[36] J. Reignier, F. Méchin, A. Sarbu, Chemical gradients in PIR foams as probed by ATR-FTIR analysis and consequences on fire resistance, Polym. Test. 93 (2021) 106972, doi:10.1016/j.polymertesting.2020.106972.
[37] S. Radice, S. Turri, M. Scicchitano, Fourier transform infrared studies on deblocking and crosslinking mechanisms of some fluorine containing monocomponent polyurethanes, Appl. Spectrosc. 58 (2004) 535–542, doi:10.1366/000370204774103354.
[38] B. Smith, Organic nitrogen compounds IX: Urethanes and diisocyanates, Spectroscopy 35 (2020) 17–21.
[39] A. Hogg, S. Uhl, F. Feuvrier, Y. Girardet, B. Graf, T. Aellen, H. Keppner, Y. Tardy, J. Burger, Protective multilayer packaging for long-term implantable medical devices, Surf. Coatings Technol. 255 (2014) 124–129, doi:10.1016/j.surfcoat.2014.02.070.
[40] E. Herth, R. Zeggari, J.Y. Rauch, F. Remy-Martin, W. Boireau, Investigation of amorphous SiO_x layer on gold surface for Surface Plasmon Resonance measurements, Microelectron. Eng. 163 (2016) 43–48, doi:10.1016/j.mee.2016.04.014.
[41] J. Li, B. Wang, K. Chen, X. Tian, J. Zeng, J. Xu, W. Gao, The use of lignin as cross-linker for polyurethane foam for potential application in adsorbing materials, BioResources 12 (2017) 8653–8671, doi:10.15376/biores.12.4.8653-8671.
[42] S.C. Feifel, F. Lisdat, Silica nanoparticles for the layer-by-layer assembly of fully electro-active cytochrome *c* multilayers, J. Nanobiotechnology. 9 (2011) 59, doi:10.1186/1477-3155-9-59.
[43] S.H. Liu, M.Y. Shen, C.F. Kuan, H.C. Kuan, C.Y. Ke, C.L. Chiang, Improving thermal stability of polyurethane through the addition of hyperbranched polysiloxane, Polymers 11 (2019) 697, doi:10.3390/polym11040697.

[44] R.A. Majida, F.S.M. Akhirb, S.K. Ghazalib, Z. Mohamadb, Thermal stability and compression strength of rigid polyurethane/kenaf fibre biocomposite foam, Chem. Eng. (2020) 78, doi:10.3303/CET2078063.
[45] J. Karger-Kocsis, T. Bárány, Single-polymer composites (SPCs): Status and future trends, Compos. Sci. Technol. 92 (2014) 77–94, doi:10.1016/j.compscitech.2013.12.006.
[46] Y. Swolfs, I. Verpoest, L. Gorbatikh, Maximizing the hybrid effect in unidirectional hybrid composites, Mater. Des. 93 (2016) 39–45, doi:10.1016/j.matdes.2015.12.137.
[47] M.L. Costa, M.C. Rezende, S.F.M. De Almeida, Effect of void content on the moisture absorption in polymeric composites, Polym. Plast. Technol. Eng. 45 (2006) 691–698, doi:10.1080/03602550600609549.
[48] A.E. Tiuc, H. Vermeşan, T. Gabor, O. Vasile, Improved sound absorption properties of polyurethane foam mixed with textile waste, Energy Procedia 85 (2016) 559–565, doi:10.1016/j.egypro.2015.12.245.
[49] A. Kairytė, M. Kirpluks, A. Ivdre, U. Cabulis, S. Vėjelis, G. Balčiūnas, Paper waste sludge enhanced eco-efficient polyurethane foam composites: Physical–mechanical properties and microstructure, Polym. Compos. 39 (2018) 1852–1860, doi:10.1002/pc.24138.
[50] A.H. Shaik, C. Patel, A. Rahaman, S. Chakraborty, S. Kumar, S. Agashe, M. Rahaman, G. Periyasami, M.R. Chandan, Foam stability and thermo-mechanical properties of micro/nano filler loaded castor oil based flexible polyurethane foam, Mater. Res. Express. 11 (2024) 015302, doi:10.1088/2053-1591/ad19b1.